



Semi analytical study for Jeffery-Hamel flow using Shehu HPM and Elzaki HPM – A comparative study

Mamta Kapoor*

Marwadi University Research Center, Department of Mathematics, Faculty of Engineering & Technology, Marwadi University, Rajkot, 360003, Gujarat, India.

Abstract

Via this study discussion about Jeffery-Hamel fluid flow is provided including fluid flow in converging/diverging channels, influenced by Reynolds number and Hartmann number. Two innovative semi-analytical techniques are introduced, referred to as the Shehu-HPM and Elzaki-HPM methods, to analyze the solution profiles of a model governing Jeffrey-Hamel fluid flow. These methods are developed by combining the Shehu transform with the Homotopy Perturbation Method (HPM), referred to as Method I, and the Elzaki transform with HPM, referred to as Method II. The performance of these techniques is evaluated under varying parameters, including the Reynolds number and the Hartmann number. These approaches are straightforward to implement and avoid the errors typically associated with discretization or quasi-linearization. Given the increasing demand for reliable solutions to fluid mechanics models, the proposed methods offer a valuable and practical alternative for solving such problems. Their simplicity and accuracy make them particularly suitable for a wide range of applications in this field. The novelty of this work lies in the hybridization of Shehu and Elzaki transforms with HPM, addressing gaps in latest literature via providing novel techniques to address complex nonlinear fluid flow problems with improved accuracy and efficiency.

Keywords. Shehu HPM, Elzaki HPM, Jefferey-Hamel fluid flow.

2010 Mathematics Subject Classification. 35Qxx, 34Axx, 37Mxx.

Nomenclature:

Re – Reynolds number

Ha – Hartmann number

$u(r, \theta)$ - radial velocity

B_0 - electromagnetic induction

σ - electrical conductivity of the fluid

P - fluid pressure

ρ - constant fluid density

ν - kinematic viscosity parameter

α – angle between two channels

Graphical Abstract

- Formulation of the considered fluid flow problem.
- Fusion of Elzaki transform and Homotopy perturbation method to create Method I.
- Fusion of Elzaki transform and Homotopy perturbation method to create Method II.
- Implementation of Method I and Method II upon the fluid flow problem.
- The generation of the series approximation and validation/graphical significance via graphs.

Received: 26 November 2024; Accepted: 10 April 2025.

* Corresponding author's Email: mamtakapoor.78@yahoo.com .

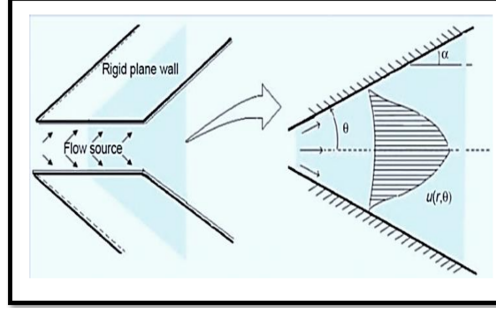


FIGURE 1. Geometry of Jeffery-Hamel flow [40].

1. INTRODUCTION

Nonlinear ordinary differential equations (NODEs) hold significant importance across various fields of engineering and applied sciences, as they are central to modeling a wide range of real-world phenomena. These equations are widely used to represent complex systems in areas such as fluid mechanics, physics, chemical processes, biology, and electrostatics. However, finding exact solutions to nonlinear problems is often challenging, and in many cases, it may not be feasible. Consequently, researchers and practitioners are continually driven to develop efficient numerical and approximate methods to tackle these problems effectively, bridging the gap between theory and practical application. Jeffery-Hamel flow is a classical solution to the Navier-Stokes equations that describes the steady, two-dimensional flow of an incompressible fluid through a converging or diverging channel. This flow is characterized by its dependence on the geometry of the channel and the nature of the boundary conditions, making it an essential model for understanding fluid dynamics in wedge-like geometries. The Jeffery-Hamel flow was first formulated by Geoffrey B. Jeffery in 1915 and later extended by Georg Hamel in 1916. Their combined efforts provided an analytical framework for solving the Navier-Stokes equations under axisymmetric and planar configurations. The solution assumes a Newtonian fluid with constant viscosity, governed by a balance of inertial, viscous, and pressure forces within a channel formed by two plane walls meeting at an angle. While original formulation applies to Newtonian fluids, researchers have adapted Jeffery-Hamel flow to investigate non-Newtonian fluids. These studies incorporate constitutive models, such as power-law, Bingham plastic, or Carreau models, to account for the complex rheological properties of fluids like polymers, suspensions, and biological fluids. Such extensions expand its applicability to real-world scenarios where the assumption of constant viscosity does not hold.

Jeffery Hamel flow provides the motion of a viscous, incompressible flow of fluid between two inclined walls. These walls may converge or diverge accordingly. In such fluid flow, the flow occurs between the walls having angle 2α which created converging or diverging channel. Such flow is mainly considered in the polar form due to the radial nature of the channel. The governing equations of the Jeffery Hamel fluid flow are derived with the aid of Navier Stokes equation and continuity equation which are adapted for the polar coordinates. Via the continuity equation, mass conservation is handled whereas due to the radial and tangential momentum equations pressure forces, viscous effects, and inertial forces are tackled. Some of the latest references related to proposed work are provided in [1, 43].

The Mathematical Formulation of Jeffrey Hamel's Flow Problem The Jeffery-Hamel flow problem, described by a nonlinear ordinary differential equation (NODE), models the steady, two-dimensional flow of a viscous, conductive, and incompressible fluid at the intersection of two rigid, non-parallel plane walls that meet at an angle of 2α . The flow is assumed to be perfectly radial and symmetric, meaning the velocity field is exclusively in the radial direction and varies with r and θ . The geometry of the concerned model is presented via Figure 1.

The continuity equation and Navier-Stokes equations can be formulated in polar coordinates as [40]:

$$\frac{\rho}{r} \frac{\partial}{\partial r} (ru(r, \theta)) = 0, \quad (1.1)$$

$$u(r, \theta) \frac{\partial}{\partial r} (u(r, \theta)) = -\frac{1}{\rho} \frac{\partial P}{\partial r} + \nu \left[\frac{\partial^2 u(r, \theta)}{\partial r^2} + \frac{1}{r} \frac{\partial u(r, \theta)}{\partial r} + \frac{1}{r^2} \frac{\partial^2 u(r, \theta)}{\partial \theta^2} - \frac{u(r, \theta)}{r^2} \right] - \frac{\sigma B_0^2}{\rho r^2} u(r, \theta), \quad (1.2)$$

$$-\frac{1}{\rho r} \frac{\partial P}{\partial \theta} + \frac{2\nu}{r^2} \frac{\partial u(r, \theta)}{\partial \theta} = 0. \quad (1.3)$$



Here, $u(r, \theta)$ represents the radial velocity, B_0 denotes the electromagnetic induction, σ is the electrical conductivity of the fluid, P refers to the fluid pressure, ρ is the constant fluid density, and ν is the kinematic viscosity parameter.

Modified form of (1.1) is:

$$g(\theta) = ru(r, \theta). \quad (1.4)$$

Via considering the dimensionless parameters.

$$w(\eta) = \frac{g(\theta)}{g_{\max}}, \quad \text{where} \quad \eta = \frac{\theta}{\alpha}. \quad (1.5)$$

Via eliminating term P from (1.2) and (1.3) and utilizing (1.4) and (1.5) respectively, a third order non-linear ODE will be obtained as follows:

$$f'''(\eta) + 2\alpha \text{Re} f(\eta)f'(\eta) + (4 - \text{Ha})\alpha^2 f'(\eta) = 0. \quad (1.6)$$

B.C.s:

$$w(0) = 1, \quad w'(0) = 0, \quad w(1) = 0.$$

Provided $\text{Re} = \frac{\alpha U_{\max}}{\nu}$, and $\text{Ha}^2 = \frac{\sigma B_0^2}{\rho \nu}$, Re is the Reynolds number and Ha is Hartmann number.

Given the extensive applicability of fluid mechanics across diverse fields, researchers have developed and applied various techniques to address challenges in these areas. The following studies highlight notable contributions to the investigation of Jeffery-Hamel flow using various analytical and numerical techniques. Adel et al. [5] proposed a numerical approach for simulating the nonlinear MHD Jeffery-Hamel flow problem. Asghar et al. [9] conducted a numerical study on boundary stresses in Jeffery-Hamel flow, considering the effects of Soret and Dufour phenomena. AL-Jawary and Nabi [33] implemented three iterative methods for solving the Jeffery-Hamel flow problem. Kamran et al. [21] utilized a finite difference method (FDM) approach to perform critical value analysis for Jeffery-Hamel flow in an inclined channel, incorporating microrotations. Kumbinarasaiah and Raghunatha [28] applied a wavelet-based numerical solution for Jeffery-Hamel flow, specifically using the Hermite Wavelet Method. Jasim [20] introduced a new analytical study of nanofluid flow between two non-parallel plane walls, extending the analysis of Jeffery-Hamel flow. Vivek and Kumar [44] employed the Bernoulli wavelet approach for the numerical solution of the Jeffery-Hamel flow problem. Rezaee et al. [41] investigated heat transfer in the Jeffery-Hamel flow of a yield-stress fluid. Bisal and Chakraverty [11] explored the Jeffery-Hamel flow of nanofluids in the presence of a magnetic field, using a new approach within the Optimal Homotopy Analysis Method. Kumbinarasaiah et al. [29] analyzed Jeffery-Hamel flow and heat transfer in Eyring-Powell fluid using the Bernoulli wavelet collocation method. Hafeez et al. [17] examined the Jeffery-Hamel flow of hybrid nanofluids in convergent and divergent channels, focusing on heat transfer characteristics. Bisal et al. [12] applied the Homotopy Perturbation Method in the inverse analysis of the Jeffery-Hamel flow problem. Boudjemline et al. [13] extended the analysis of Jeffery-Hamel flow to include the thermal behavior of Oldroyd-B nanofluid in an expanding channel. El-Shenawy et al. [14] solved the MHD Jeffery-Hamel problem involving flow between two non-parallel plates, with an application to blood flow, using B-spline and Bernstein polynomial collocation approaches. They concluded that the Bernstein polynomial collocation method was more efficient and accurate than the B-spline collocation approach. These studies collectively showcase the diverse methodologies and innovative approaches undertaken to address the complexities of Jeffery-Hamel flow across various physical and engineering aspects. Some of the useful and relevant research is mentioned in [34]-[30]. Semi-analytical techniques, such as the Shehu Homotopy Perturbation Method (Shehu HPM) and the Elzaki Homotopy Perturbation Method (Elzaki HPM), have emerged as powerful tools for solving nonlinear differential equations, particularly in fluid dynamics and related fields. These methods combine the strengths of the Homotopy Perturbation Method (HPM) with integral transforms, enhancing their efficiency and accuracy in handling complex boundary value problems. The Shehu HPM integrates Shehu transform with the perturbation method, providing a systematic approach to simplify and solve problems with intricate nonlinearities by mapping them into more manageable domains. Similarly, the Elzaki HPM employs the Elzaki transform, offering rapid convergence and reliable solutions while reducing computational complexity. These techniques have shown promise in addressing challenging problems such as the Jeffery-Hamel flow, where traditional numerical methods may falter due to instability or computational intensity. Their adaptability and effectiveness in yielding approximate yet accurate solutions make them highly valuable for researchers exploring fluid mechanics and other applied sciences. Via Tables 1 and 2, the basic properties of Shehu and Elzaki transforms are provided. Via the Shehu HPM the classical Homotopy perturbation method is enhanced. These are many advantages of Shehu HPM over other methods such as; It can efficiently handle the high-order non-linearities without any need of linearization. It converges faster to the closed form of solution. It simplifies the solution process that is why it is more time-efficient. In this method there is no scope of discretization related error. Via Tables 1 and 2, the basic properties of Shehu and Elzaki transform are provided respectively.



Shehu Transform.

Definition 1.1. [24]

$$S[f(t)] = \int_0^{\infty} \exp\left(-\frac{st}{\nu}\right) f(t) dt, \quad (1.7)$$

$$S[f'(t)] = \frac{s}{\nu} S[f(t)] - f(0), \quad (1.8)$$

$$S[f''(t)] = \frac{s^2}{\nu^2} S[f(t)] - \frac{s}{\nu} f(0) - f'(0), \quad (1.9)$$

$$S[f'''(t)] = \frac{s^3}{\nu^3} S[f(t)] - \frac{s^2}{\nu^2} f(0) - \frac{s}{\nu} f'(0) - f''(0), \quad (1.10)$$

$$S[f^{(n)}(t)] = \frac{s^n}{\nu^n} S[f(t)] - \frac{s^{n-1}}{\nu^{n-1}} f(0) - \frac{s^{n-2}}{\nu^{n-2}} f'(0) - \dots - f^{(n-1)}(0). \quad (1.11)$$

Serial Number	$f(t)$	$S[f(t)]$
1	1	$\frac{\nu}{s}$
2	t	$\frac{\nu^2}{s^2}$
3	t^2	$\frac{2\nu^3}{s^3}$
4	t^3	$\frac{6\nu^4}{s^4}$
6	e^{at}	$\frac{\nu}{s-a\nu}$
7	$\sin(at)$	$\frac{a\nu^2}{s^2+a^2\nu^2}$
8	$\cos(at)$	$\frac{s\nu}{s^2+a^2\nu^2}$
9	$\sinh(at)$	$\frac{a\nu^2}{s^2-a^2\nu^2}$
10	$\cosh(at)$	$\frac{s\nu}{s^2-a^2\nu^2}$

TABLE 1. Shehu transform of diversified functions

Elzaki HPM is very simple to implement upon a wide range of linear and non-linear differential equations. It provides closed form of exact solutions effectively for moderately non-linear differential equations. It converges faster for simple or mild non-linear models. Unlike traditional numerical method it does not require any sort of discretization of linearization.

Elzaki Transform of function: Elzaki transform is defined as follows [15]:

$$E(\nu) = \nu \int_0^{\infty} f(t) e^{-\frac{t}{\nu}} dt. \quad (1.12)$$

Where $f(t)$ is considered as the time function.

$$E[u_t(x, t)] = \frac{1}{\nu} E[u(x, t)] - \nu u(x, 0), \quad (1.13)$$

$$E[u_t(x, y, t)] = \frac{1}{\nu} E[u(x, y, t)] - \nu u(x, y, 0), \quad (1.14)$$

$$E[u_t(x, y, z, t)] = \frac{1}{\nu} E[u(x, y, z, t)] - \nu u(x, y, z, 0). \quad (1.15)$$

The latest developments in the application of Shehu and Elzaki and related transform-based techniques are outlined below. Kapoor and Joshi [22] conducted a comparative study of the Sumudu Homotopy Perturbation Method (HPM) and the Elzaki HPM for solving coupled Burgers' equations. Kapoor et al. [23] investigated the fractional telegraph equation using the Shehu Homotopy Perturbation Method. Kelil and Appadu [26] implemented the Shehu-Adomian Decomposition Method for solving dispersive KdV-type equations. Ahmed [6] applied the Jafari Variation Iteration Method to solve the one-dimensional fractional diffusion equation. Kapoor et al. [24] proposed an analytical approach for solving the fractional hyperbolic telegraph equation using the Shehu transform in one, two, and three dimensions. Oderinu et al. [40] presented solutions to the nonlinear Brusselator model using a combined Sawi transform and Homotopy Analysis Method. Oderinu et al. [?] provided solutions to partial differential equations using a deformation-based Sawi transform approach. Kapoor [25] utilized the Sumudu Transform



TABLE 2. Elzaki transform of the specified functions.

$f(t)$	$E[f(t)] = T(\nu)$
1	ν^2
t	ν^3
t^n	$n\nu^{n+2}$
e^{at}	$\frac{\nu^2}{1-a\nu}$
$\sin(at)$	$\frac{a\nu^3}{1+a^2\nu^2}$
$\cos(at)$	$\frac{a\nu^2}{1+a^2\nu^2}$
$\sinh(at)$	$\frac{a\nu^3}{1-a^2\nu^2}$
$\cosh(at)$	$\frac{a\nu^2}{1-a^2\nu^2}$

Iterative Method for solving linear and non-linear time-fractional Schrödinger equations. Liaquat [31] explored approximate and exact solutions to some nonlinear differential equations using a novel coupling approach within the framework of conformable fractional derivatives. Alsidrani [8] delivered a comprehensive review of recent numerical methods for solving fractional partial differential equations (FPDEs). Liaquat et al. [32] derived series and closed-form solutions for Caputo time-fractional wave and heat problems with variable coefficients using a novel approach. Kshirsagar [27] proposed an innovative computational approach for solving fuzzy space-time fractional telegraph equation using the new iterative transform method.

Novelty/Originality of the proposed research. There exist several originalities for implementing these techniques but some of them are notified ahead.

- Hybridization of novel integration transforms with HPM
- Comparative analysis of two proposed methods
- Avoidance of common numerical methods errors such as; discretization/linearization/quasi-linearization
- Extension to MHD flows

Research questions related to proposed work.

- **What is Already Known in the Open Literature?**
 Reply - Homotopy Perturbation Method (HPM), Jeffrey-Hamel Flow Studies, Integral Transforms.
- **What is Missing (Research Gaps)?** Reply - Limited Exploration of Shehu and Elzaki Transforms in Nonlinear Problems, Lack of Comparative Analysis, MHD Applications, avoidance of discretization errors.
- **What Needs to be Done and Why?** Reply - To develop and compare hybrid analytical methods (Shehu HPM vs. Elzaki HPM). To address nonlinear boundary conditions. To provide a comprehensive error and convergence analysis.

Main Motivations of the Study. The main motivation of using these techniques is to tackle complex-natured fluid flow problems without using any sort of discretization/linearization/quasi-linearization. So that there is no scope for such related errors. Moreover, these techniques are very time-efficient and computational cost is less as compare to the traditional numerical methods.

Limitations of the proposed techniques. There are some limitations also of the proposed techniques such as:

- The accuracy and convergence of Shehu HPM rely upon choice of initial approximation. A poor initial guess can be the reason for slow convergence.
- Elzaki HPM may not be capable to tackle highly nonlinear differential equations efficiently, or it might converge slower as compared to Shehu HPM or it might require additional terms to achieve accuracy.

2. IMPLEMENTATION OF PROPOSED REGIMES

METHOD I – Shehu HPM. Applying Shehu transform upon (1.6):

$$S[f'''(\eta)] = -S [2\alpha Re f(\eta)f'(\eta) + (4 - Ha)\alpha^2 f'(\eta)] ,$$

$$\left(\frac{s}{\nu}\right)^3 S[f(\eta)] - \left(\frac{s}{\nu}\right)^2 f(0) - \left(\frac{s}{\nu}\right) f'(0) - f''(0) = -S [2\alpha Re f(\eta)f'(\eta) + (4 - Ha)\alpha^2 f'(\eta)] .$$



Considered $f''(0) = c$.

$$\begin{aligned} \left(\frac{s}{\nu}\right)^3 S[f(\eta)] - \left(\frac{s}{\nu}\right)^2 - c &= -S [2\alpha\text{Re} f(\eta)f'(\eta) + (4 - \text{Ha})\alpha^2 f'(\eta)], \\ \left(\frac{s}{\nu}\right)^3 S[f(\eta)] &= \left[\left(\frac{s}{\nu}\right)^2 + c\right] - S [2\alpha\text{Re} f(\eta)f'(\eta) + (4 - \text{Ha})\alpha^2 f'(\eta)], \\ S[f(\eta)] &= \left(\frac{\nu}{s}\right)^3 \left[\left(\frac{s}{\nu}\right)^2 + c\right] - \left(\frac{\nu}{s}\right)^3 S [2\alpha\text{Re} f(\eta)f'(\eta) + (4 - \text{Ha})\alpha^2 f'(\eta)], \\ f(\eta) &= S^{-1} \left[\left(\frac{\nu}{s}\right)^3 \left(\left(\frac{s}{\nu}\right)^2 + c\right)\right] - S^{-1} \left[\left(\frac{\nu}{s}\right)^3 S [2\alpha\text{Re} f(\eta)f'(\eta) + (4 - \text{Ha})\alpha^2 f'(\eta)]\right], \\ f(\eta) &= S^{-1} \left(\frac{\nu}{s}\right) + cS^{-1} \left(\frac{\nu}{s}\right)^3 - S^{-1} \left[\left(\frac{\nu}{s}\right)^3 S [2\alpha\text{Re} f(\eta)f'(\eta) + (4 - \text{Ha})\alpha^2 f'(\eta)]\right], \\ f(\eta) &= \left[1 + c\frac{\eta^2}{2!}\right] - S^{-1} \left[\left(\frac{\nu}{s}\right)^3 S [2\alpha\text{Re} f(\eta)f'(\eta) + (4 - \text{Ha})\alpha^2 f'(\eta)]\right]. \end{aligned}$$

Applying HPM:

$$\sum_{n=0}^{\infty} p^n f_n(\eta) = \left[1 + c\frac{\eta^2}{2!}\right] - pS^{-1} \left[\left(\frac{\nu}{s}\right)^3 S \left(2\alpha\text{Re} \sum_{n=0}^{\infty} p^n A_n(\eta) + (4 - \text{Ha})\alpha^2 \sum_{n=0}^{\infty} p^n f'_n(\eta)\right)\right].$$

Considered

$$\begin{aligned} f(\eta) &= \sum_{n=0}^{\infty} p^n f_n(\eta), \\ f(\eta)f'(\eta) &= \sum_{n=0}^{\infty} p^n A_n(\eta). \end{aligned}$$

Comparing p^0 :

$$f_0(\eta) = \left[1 + c\frac{\eta^2}{2!}\right].$$

Comparing p^1 :

$$f_1 = -pS^{-1} \left[\left(\frac{\nu}{s}\right)^3 S (2\alpha\text{Re} A_0 + (4 - \text{Ha})\alpha^2 f'_0)\right],$$

where

$$A_0(\eta) = f_0(\eta)f'_0(\eta) = c\eta + \frac{c^2\eta^3}{2}.$$

$$\begin{aligned} f_1(\eta) &= -S^{-1} \left[\left(\frac{\nu}{s}\right)^3 S \left[2\alpha\text{Re} \left(c\eta + \frac{c^2\eta^3}{2}\right) + (4 - \text{Ha})\alpha^2 c\eta\right]\right], \\ f_1(\eta) &= -S^{-1} \left[\left(\frac{\nu}{s}\right)^3 \left[2\alpha\text{Re} \left(cS[\eta] + \frac{c^2}{2}S[\eta^3]\right) + (4 - \text{Ha})\alpha^2 cS[\eta]\right]\right], \\ f_1(\eta) &= -S^{-1} \left[\left(\frac{\nu}{s}\right)^3 \left[2\alpha\text{Re} \left(c\left(\frac{\nu}{s}\right)^2 + \frac{c^2}{2} \cdot 3! \left(\frac{\nu}{s}\right)^4\right) + (4 - \text{Ha})\alpha^2 c\left(\frac{\nu}{s}\right)^2\right]\right], \\ f_1(\eta) &= -S^{-1} \left[2\alpha\text{Re} \left(c\left(\frac{\nu}{s}\right)^5 + \frac{c^2}{2} \cdot 3! \left(\frac{\nu}{s}\right)^7\right) + (4 - \text{Ha})\alpha^2 c\left(\frac{\nu}{s}\right)^5\right], \\ f_1(\eta) &= -\left[2\alpha\text{Re} \left(cS^{-1} \left(\frac{\nu}{s}\right)^5 + \frac{c^2}{2} \cdot 3!S^{-1} \left(\frac{\nu}{s}\right)^7\right) + (4 - \text{Ha})\alpha^2 cS^{-1} \left(\frac{\nu}{s}\right)^5\right], \\ f_1(\eta) &= -\left[2\alpha\text{Re} \left(c\frac{\eta^4}{4!} + \frac{c^2}{2} \cdot 3!\frac{\eta^6}{6!}\right) + (4 - \text{Ha})\alpha^2 c\frac{\eta^4}{4!}\right], \\ f_1(\eta) &= -\left[2\alpha\text{Re} \left(c\frac{\eta^4}{4!} + 3c^2\frac{\eta^6}{6!}\right) + (4 - \text{Ha})\alpha^2 c\frac{\eta^4}{4!}\right]. \end{aligned}$$



$$\begin{aligned}
 M_1 &= 2\alpha \text{Re } c, \\
 M_2 &= 6\alpha \text{Re } c^2, \\
 M_3 &= (4 - \text{Ha})\alpha^2 c. \\
 f_1(\eta) &= - \left[\frac{M_1 \eta^4}{4!} + \frac{M_2 \eta^6}{6!} + \frac{M_3 \eta^4}{4!} \right], \\
 f_1(\eta) &= - \left[\frac{M_1 + M_3}{4!} \eta^4 + \frac{M_2}{6!} \eta^6 \right].
 \end{aligned}$$

Comparing p^2 :

$$\begin{aligned}
 f_2(\eta) &= -S^{-1} \left[\left(\frac{\nu}{s}\right)^3 S (2\alpha \text{Re } A_1(\eta) + (4 - \text{Ha})\alpha^2 f_1'(\eta)) \right]. \\
 f_2(\eta) &= -S^{-1} \left[\left(\frac{\nu}{s}\right)^3 S [2\alpha \text{Re } A_1(\eta) + (4 - \text{Ha})\alpha^2 f_1'(\eta)] \right]. \tag{2.1}
 \end{aligned}$$

Calculation:

$$\begin{aligned}
 f_1'(\eta) &= - \left[\frac{(M_1 + M_3)\eta^3}{3!} + \frac{M_2\eta^5}{5!} \right], \\
 A_1(\eta) &= f_1(\eta)f_0'(\eta) + f_0(\eta)f_1'(\eta), \\
 A_1(\eta) &= \left[\frac{(M_1 + M_3)c\eta^5}{4!} + \frac{cM_2\eta^7}{6!} \right] + \left[\frac{(M_1 + M_3)\eta^3}{3!} + \frac{M_2\eta^5}{5!} + \frac{c(M_1 + M_3)}{2} \frac{\eta^5}{3!} + \frac{cM_2}{2} \frac{\eta^7}{5!} \right], \\
 f_2(\eta) &= -S^{-1} \left[\left(\frac{\nu}{s}\right)^3 S \left(-2\alpha \text{Re} \left[\frac{(M_1 + M_3)c\eta^5}{4!} + \frac{cM_2\eta^7}{6!} \right] \right. \right. \\
 &\quad \left. \left. + \left[\frac{(M_1 + M_3)\eta^3}{3!} + \frac{M_2\eta^5}{5!} + \frac{c(M_1 + M_3)}{2} \frac{\eta^5}{3!} + \frac{cM_2}{2} \frac{\eta^7}{5!} \right] \right) \right. \\
 &\quad \left. + (4 - \text{Ha})\alpha^2 \left[- \left(\frac{(M_1 + M_3)\eta^3}{3!} + \frac{M_2\eta^5}{5!} \right) \right] \right], \\
 f_2(\eta) &= S^{-1} \left[\left(\frac{\nu}{s}\right)^3 \left[2\alpha \text{Re} \left[\frac{(M_1 + M_3)c}{4!} \cdot S[\eta^5] + \frac{cM_2}{6!} \cdot S[\eta^7] \right] \right. \right. \\
 &\quad \left. \left. + \left[\frac{(M_1 + M_3)}{3!} S[\eta^3] + \frac{M_2}{5!} S[\eta^5] + \frac{c(M_1 + M_3)}{2} \frac{S[\eta^5]}{3!} + \frac{cM_2}{2} \frac{S[\eta^7]}{5!} \right] \right) \right. \\
 &\quad \left. + (4 - \text{Ha})\alpha^2 \left[\frac{(M_1 + M_3)}{3!} S[\eta^3] + \frac{M_2}{5!} S[\eta^5] \right] \right], \\
 f_2(\eta) &= S^{-1} \left[2\alpha \text{Re} \left[\frac{(M_1 + M_3)c}{4! \cdot 5!} \left(\frac{\nu}{s}\right)^9 + \frac{cM_2}{6! \cdot 7!} \left(\frac{\nu}{s}\right)^{11} \right] \right. \\
 &\quad \left. + \left[(M_1 + M_3) \left(\frac{\nu}{s}\right)^7 + M_2 \left(\frac{\nu}{s}\right)^9 + \frac{c(M_1 + M_3)}{12} \left(\frac{\nu}{s}\right)^9 + \frac{cM_2}{240} \left(\frac{\nu}{s}\right)^{11} \right] \right. \\
 &\quad \left. + (4 - \text{Ha})\alpha^2 \left[(M_1 + M_3) \left(\frac{\nu}{s}\right)^7 + M_2 \left(\frac{\nu}{s}\right)^9 \right] \right], \\
 f_2(\eta) &= \left[2\alpha \text{Re} \left[\frac{(M_1 + M_3)c}{8!} \eta^8 + \frac{7cM_2}{10!} \eta^{10} \right] \right. \\
 &\quad \left. + \left[\frac{(M_1 + M_3)\eta^6}{6!} + \frac{M_2\eta^8}{8!} + \frac{10c(M_1 + M_3)\eta^8}{8!} + \frac{21cM_2\eta^{10}}{10!} \right] \right]
 \end{aligned}$$



$$+ (4 - \text{Ha})\alpha^2 \left[\frac{(M_1 + M_3)\eta^6}{6!} + \frac{M_2\eta^8}{8!} \right],$$

$$f(\eta) = f_0(\eta) + pf_1(\eta) + p^2f_2(\eta) + \dots.$$

Considered $p \rightarrow 1$:

$$f(\eta) = f_0(\eta) + f_1(\eta) + f_2(\eta) + \dots. \quad (2.2)$$

$$f(\eta) = \left[1 + c \frac{\eta^2}{2!} \right] - \left[\frac{M_1\eta^4}{4!} + \frac{M_2\eta^6}{6!} + \frac{M_3\eta^4}{4!} \right]$$

$$+ \left[2\alpha \text{Re} \left[\frac{(M_1 + M_3)5c\eta^8}{8!} + \frac{7cM_2\eta^{10}}{10!} \right] \right]$$

$$+ \left[\frac{(M_1 + M_3)\eta^6}{6!} + \frac{M_2\eta^8}{8!} + \frac{10c(M_1 + M_3)\eta^8}{8!} + \frac{21cM_2\eta^{10}}{10!} \right]$$

$$+ (4 - \text{Ha})\alpha^2 \left[\frac{(M_1 + M_3)\eta^6}{6!} + \frac{M_2\eta^8}{8!} \right] + \dots.$$

METHOD II – Elzaki HPM. Applying Elzaki transform upon (1.6):

$$E[f'''(\eta)] = -E [2\alpha \text{Re} f(\eta)f'(\eta) + (4 - \text{Ha})\alpha^2 f'(\eta)],$$

$$\left(\frac{1}{\nu}\right)^3 E[f(\eta)] - \left[\frac{1}{\nu}f(0) + f'(0) + \nu f''(0)\right] = -E [2\alpha \text{Re} f(\eta)f'(\eta) + (4 - \text{Ha})\alpha^2 f'(\eta)],$$

$$\left(\frac{1}{\nu}\right)^3 E[f(\eta)] - \left(\frac{1}{\nu} + \nu d\right) = -E [2\alpha \text{Re} f(\eta)f'(\eta) + (4 - \text{Ha})\alpha^2 f'(\eta)],$$

$$\left(\frac{1}{\nu}\right)^3 E[f(\eta)] = \left(\frac{1}{\nu} + \nu d\right) - E [2\alpha \text{Re} f(\eta)f'(\eta) + (4 - \text{Ha})\alpha^2 f'(\eta)],$$

$$E[f(\eta)] = \nu^3 \left(\frac{1}{\nu} + \nu d\right) - \nu^3 E [2\alpha \text{Re} f(\eta)f'(\eta) + (4 - \text{Ha})\alpha^2 f'(\eta)],$$

$$E[f(\eta)] = \nu^2 + d\nu^4 - \nu^3 E [2\alpha \text{Re} f(\eta)f'(\eta) + (4 - \text{Ha})\alpha^2 f'(\eta)],$$

$$f(\eta) = E^{-1} [\nu^2 + d\nu^4] - E^{-1} [\nu^3 E [2\alpha \text{Re} f(\eta)f'(\eta) + (4 - \text{Ha})\alpha^2 f'(\eta)]],$$

$$f(\eta) = \left[1 + d \frac{\eta^2}{2!} \right] - E^{-1} [\nu^3 E [2\alpha \text{Re} f(\eta)f'(\eta) + (4 - \text{Ha})\alpha^2 f'(\eta)]].$$

Applying HPM:

$$\sum_{n=0}^{\infty} p^n f_n(\eta) = \left[1 + d \frac{\eta^2}{2!} \right] - pE^{-1} \left[\nu^3 E \left[2\alpha \text{Re} \sum_{n=0}^{\infty} p^n B_n(\eta) + (4 - \text{Ha})\alpha^2 \sum_{n=0}^{\infty} p^n f_n(\eta) \right] \right],$$

where

$$f(\eta) = \sum_{n=0}^{\infty} p^n f_n(\eta),$$

$$f(\eta)f'(\eta) = \sum_{n=0}^{\infty} p^n B_n(\eta).$$

Comparing p^0 :

$$f_0 = \left[1 + d \frac{\eta^2}{2!} \right]. \quad (2.3)$$

Comparing p^1 :

$$f_1(\eta) = -E^{-1} [\nu^3 E [2\alpha \text{Re} B_0(\eta) + (4 - \text{Ha})\alpha^2 f'_0(\eta)]],$$



$$\begin{aligned}
 f_1(\eta) &= -E^{-1} \left[\nu^3 E \left[2\alpha \operatorname{Re} \left(d\eta + \frac{d^2}{2} \eta^3 \right) + (4 - \operatorname{Ha}) \alpha^2 d\eta \right] \right], \\
 f_1(\eta) &= -E^{-1} \left[\nu^3 \left[2\alpha \operatorname{Re} \left(dE[\eta] + \frac{d^2}{2} E[\eta^3] \right) + (4 - \operatorname{Ha}) \alpha^2 dE[\eta] \right] \right], \\
 f_1(\eta) &= -E^{-1} \left[\nu^3 \left[2\alpha \operatorname{Re} \left(d\nu^3 + \frac{d^2}{2} (3!\nu^5) \right) + (4 - \operatorname{Ha}) \alpha^2 d(\nu^3) \right] \right], \\
 f_1(\eta) &= -E^{-1} \left[2\alpha \operatorname{Re} \left(d\nu^6 + \frac{d^2}{2} (3!\nu^8) \right) + (4 - \operatorname{Ha}) \alpha^2 d(\nu^6) \right], \\
 f_1(\eta) &= -E^{-1} \left[2\alpha \operatorname{Re} \left(dE^{-1}[\nu^6] + \frac{d^2}{2} (3!E^{-1}[\nu^8]) \right) + (4 - \operatorname{Ha}) \alpha^2 d(E^{-1}[\nu^6]) \right], \\
 f_1(\eta) &= - \left[2\alpha \operatorname{Re} \left(d \frac{\eta^4}{4!} + 3d^2 \frac{\eta^6}{6!} \right) + (4 - \operatorname{Ha}) \alpha^2 d \frac{\eta^4}{4!} \right], \\
 f_1(\eta) &= - \left[2\alpha \operatorname{Re} d \frac{\eta^4}{4!} + 6\alpha \operatorname{Re} d^2 \frac{\eta^6}{6!} + (4 - \operatorname{Ha}) \alpha^2 d \frac{\eta^4}{4!} \right].
 \end{aligned}$$

Let

$$N_1 = 2\alpha \operatorname{Re} d, \tag{2.4}$$

$$N_2 = 6\alpha \operatorname{Re} d^2, \tag{2.5}$$

$$N_3 = (4 - \operatorname{Ha}) \alpha^2 d, \tag{2.6}$$

$$B_1 = f_1 f_0' + f_0 f_1'. \tag{2.7}$$

$$\begin{aligned}
 B_1(\eta) &= - \left[\frac{(N_1 + N_3)d\eta^5}{4!} + \frac{N_2d\eta^7}{6!} + \frac{(N_1 + N_3)\eta^3}{3!} + \frac{N_2\eta^5}{5!} + \frac{d\eta^2}{2} \left(\frac{(N_1 + N_3)\eta^3}{3!} + \frac{N_2\eta^5}{5!} \right) \right], \\
 B_1(\eta) &= - \left[\frac{(N_1 + N_3)d\eta^5}{4!} + \frac{N_2d\eta^7}{6!} + \frac{(N_1 + N_3)\eta^3}{3!} + \frac{N_2\eta^5}{5!} + \left(\frac{(N_1 + N_3)d\eta^5}{12} + \frac{N_2d\eta^7}{240} \right) \right]. \\
 f_1(\eta) &= - \left[\frac{N_1\eta^4}{4!} + \frac{N_2\eta^6}{6!} + \frac{N_3\eta^4}{4!} \right], \\
 f_1(\eta) &= - \left[\frac{(N_1 + N_3)\eta^4}{4!} + \frac{N_2\eta^6}{6!} \right], \\
 f_1'(\eta) &= - \left[\frac{(N_1 + N_3)\eta^3}{3!} + \frac{N_2\eta^5}{5!} \right].
 \end{aligned}$$

Comparing p^2 :

$$\begin{aligned}
 f_2(\eta) &= -E^{-1} \left[\nu^3 E \left[2\alpha \operatorname{Re} B_1 + (4 - \operatorname{Ha}) \alpha^2 f_1' \right] \right], \\
 f_2(\eta) &= -E^{-1} \left[\nu^3 E \left[2\alpha \operatorname{Re} \left[- \left(\frac{(N_1 + N_3)d\eta^5}{4!} + \frac{N_2d\eta^7}{6!} + \frac{(N_1 + N_3)\eta^3}{3!} + \frac{N_2\eta^5}{5!} + \left(\frac{(N_1 + N_3)d\eta^5}{12} + \frac{N_2d\eta^7}{240} \right) \right) \right] \right. \right. \\
 &\quad \left. \left. + (4 - \operatorname{Ha}) \alpha^2 \left[- \left(\frac{(N_1 + N_3)\eta^3}{3!} + \frac{N_2\eta^5}{5!} \right) \right] \right] \right], \\
 f_2(\eta) &= E^{-1} \left[\nu^3 E \left[2\alpha \operatorname{Re} \left[\frac{(N_1 + N_3)d\eta^5}{4!} + \frac{N_2d\eta^7}{6!} + \frac{(N_1 + N_3)\eta^3}{3!} + \frac{N_2\eta^5}{5!} + \left(\frac{(N_1 + N_3)d\eta^5}{12} + \frac{N_2d\eta^7}{240} \right) \right] \right. \right. \\
 &\quad \left. \left. + (4 - \operatorname{Ha}) \alpha^2 \left[\frac{(N_1 + N_3)\eta^3}{3!} + \frac{N_2\eta^5}{5!} \right] \right] \right],
 \end{aligned}$$



$$\begin{aligned}
f_2(\eta) &= E^{-1} \left[\nu^3 \left[2\alpha \operatorname{Re} \left[\frac{(N_1 + N_3)d5!\nu^7}{4!} + \frac{N_2d7!\nu^9}{6!} + (N_1 + N_3)\nu^5 + N_2\nu^7 \right. \right. \right. \\
&\quad \left. \left. \left. + \left(\frac{(N_1 + N_3)d5!\nu^7}{12} + \frac{N_2d7!\nu^9}{240} \right) \right] + (4 - \operatorname{Ha})\alpha^2 \left[(N_1 + N_3)\nu^5 + N_2\nu^7 \right] \right] \right], \\
f_2(\eta) &= E^{-1} \left[2\alpha \operatorname{Re} \left[(N_1 + N_3)5d\nu^{10} + N_27d\nu^{12} + (N_1 + N_3)\nu^8 + N_2\nu^{10} \right. \right. \\
&\quad \left. \left. + \left((N_1 + N_3)10d\nu^{10} + N_221d\nu^{12} \right) \right] + (4 - \operatorname{Ha})\alpha^2 \left[(N_1 + N_3)\nu^8 + N_2\nu^{10} \right] \right], \\
f_2(\eta) &= \left[2\alpha \operatorname{Re} \left[(N_1 + N_3)\frac{5d\eta^8}{8!} + N_2\frac{7d\eta^{10}}{10!} + \frac{(N_1 + N_3)\eta^6}{6!} + \frac{N_2\eta^8}{8!} \right. \right. \\
&\quad \left. \left. + \left((N_1 + N_3)\frac{10d\eta^8}{8!} + N_2\frac{21d\eta^{10}}{10!} \right) \right] + (4 - \operatorname{Ha})\alpha^2 \left[\frac{(N_1 + N_3)\eta^6}{6!} + \frac{N_2\eta^8}{8!} \right] \right], \\
f(\eta) &= f_0(\eta) + pf_1(\eta) + p^2f_2(\eta) + \dots
\end{aligned}$$

Considered $p \rightarrow 1$:

$$\begin{aligned}
f(\eta) &= f_0(\eta) + f_1(\eta) + f_2(\eta) + \dots, \\
f(\eta) &= \left[1 + d\frac{\eta^2}{2!} \right] - \left[\frac{(N_1 + N_3)\eta^4}{4!} + \frac{N_2\eta^6}{6!} \right] \\
&\quad + \left[2\alpha \operatorname{Re} \left[\frac{(N_1 + N_3)5d\eta^8}{8!} + \frac{N_27d\eta^{10}}{10!} + \frac{(N_1 + N_3)\eta^6}{6!} + \frac{N_2\eta^8}{8!} \right. \right. \\
&\quad \left. \left. + \left(\frac{(N_1 + N_3)10d\eta^8}{8!} + \frac{N_221d\eta^{10}}{10!} \right) \right] + (4 - \operatorname{Ha})\alpha^2 \left[\frac{(N_1 + N_3)\eta^6}{6!} + \frac{N_2\eta^8}{8!} \right] \right] + \dots
\end{aligned}$$

3. GRAPHICAL ANALYSIS RAPHICAL ANALYSIS

The robust analysis of the solution graphs at different parameters is provided in this section.

Analysis of Solution Profiles Based on Parameters. From Figure 2, it is evident that reducing the angle α (with $\alpha < 0$) results in a decreased solution profile. Similarly, Figure 3 demonstrates that increasing the angle α (with $\alpha > 0$) also leads to a reduction in the solution profile. A consistent trend is observed in Figure 4, where a decrease in α ($\alpha < 0$) results in a diminished solution profile. In Figure 5, an increase in α ($\alpha > 0$) similarly leads to a reduced solution profile.

Moving on to the effect of the Reynolds number (Re), Figure 6 to Figure 8 indicate that increasing Re results in a reduction of the solution profile. However, a contrasting behavior is observed in Figure 9, where an increase in Re leads to an enhanced solution profile. This trend is reaffirmed in Figures 10 and 11, where higher values of Re are associated with an increase in the solution profile.

The influence of the Hartmann number (Ha) is illustrated in Figure 12 to Figure 14, where increasing Ha leads to a decrease in the solution profile. Interestingly, Figures 15 and 16 present an opposite trend, showing that higher Ha results in an elevated solution profile. However, Figure 17 returns to the initial trend, with increasing Ha reducing the solution profile.

Returning to the role of the angle α , Figure 18 shows that decreasing α ($\alpha < 0$) lowers the solution profile, while Figure 19 suggests that increasing α ($\alpha > 0$) similarly diminishes the solution profile. Figures 20 and 21 confirm these observations, demonstrating that reductions in α ($\alpha < 0$) and increases in α ($\alpha > 0$) result in reduced solution profiles.

The analysis of the Reynolds number continues in Figure 22, where a lower Re corresponds to a decreased solution profile. Conversely, Figures 23 and 24 show that increasing Re reduces the solution profile. However, Figure 25 to Figure 27 highlight cases where higher values of Re enhance the solution profile, particularly for larger values.

The Hartmann number's impact is revisited in Figure 28 to Figure 30, which reveal that increasing Ha reduces the solution profile. Yet, Figures 31 and 32 demonstrate that a higher Ha can also lead to an increase in the solution profile. Finally, Figure 33 confirms that incrementing Ha can result in a decline in the solution profile.



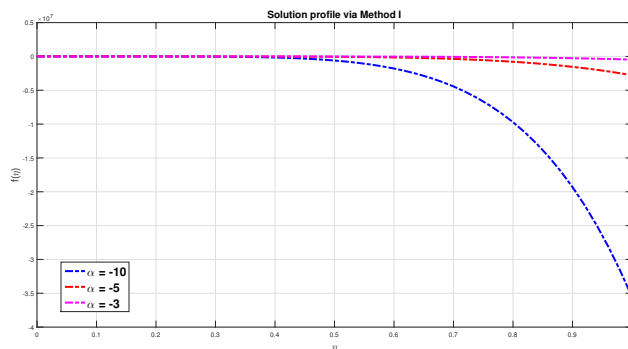


FIGURE 2. Solution profile at $\alpha = -10, -5, -3$ with $Re = 1000, Ha = 1000, N = 51$ via Method I.

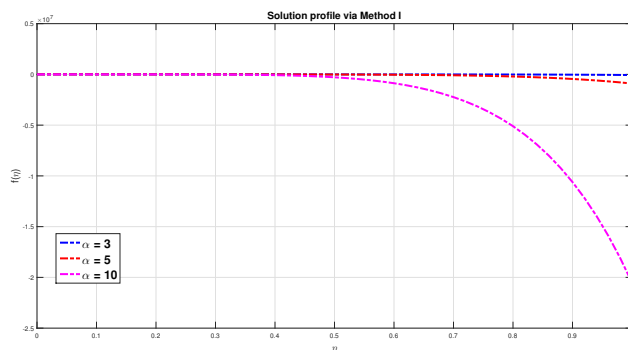


FIGURE 3. Solution profile at $\alpha = 3, 5, 10$ with $Re = 1000, Ha = 1000, N = 51$ via Method I.

As per Figure 2, soliton behaviors will be: $\alpha = -10$: Dark soliton, $\alpha = -5$: Gray soliton, $\alpha = -3$: Bright soliton or near-zero perturbation. As per Figure 3, soliton behaviors will be: $\alpha = 10$: Dark soliton, $\alpha = 5$: Gray soliton, $\alpha = 3$: Bright soliton or near-zero perturbation.

As per Figure 4, soliton behaviors will be: $\alpha = -3.5$: Dark soliton, $\alpha = -2.5$: Gray soliton, $\alpha = -1.5$: Bright soliton or near-zero perturbation. As per Figure 5, soliton behaviors will be: $\alpha = 3.5$: Dark soliton, $\alpha = 2.5$: Gray soliton, $\alpha = 1.5$: Bright soliton or near-zero perturbation. Similarly, the soliton behavior can be tested for the other figures as well.

Main crux of the analysis.

- As the angle α becomes less negative (increasing from -10 to -3), the flow solution profile generally shows a decrease in the magnitude of deviation from the baseline. This indicates a smoother or less pronounced flow variation.
- As α increases (from 3 to 10), the solution profile is expected to show progressively larger deviations, becoming more pronounced and peaked. A larger angle enhances the divergence of the flow, leading to greater variations in velocity and pressure distribution.
- As Re increases, the inertial effects dominate over viscous forces, leading to more pronounced variations in the solution profile. Higher Re corresponds to greater momentum in the flow, amplifying peaks and troughs in the velocity and pressure distribution.

Physical significance of the results:

Observation 1. Via Figures 2 and 4, it is observed that for negative α and large value of Reynold number Re and Hartmann number Ha , when there is increase in the value of α , the solution profile got increased.



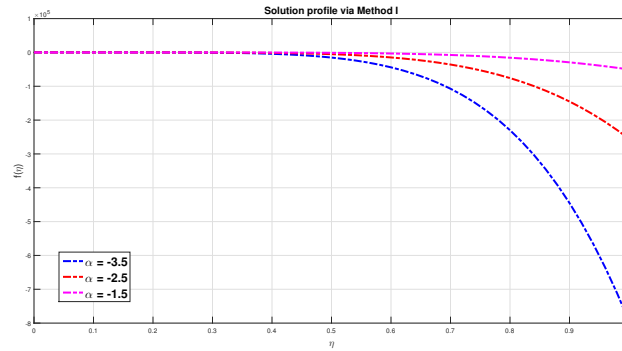


FIGURE 4. Solution profile at $\alpha = -3.5, -2.5, -1.5$ with $Re = 1000, Ha = 1000, N = 51$ via Method I.

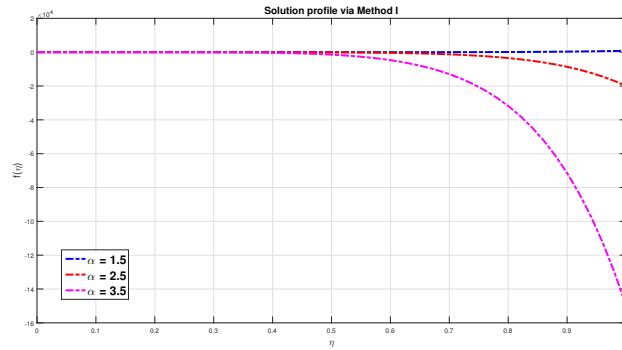


FIGURE 5. Solution profile at $\alpha = 1.5, 2.5, 3.5$ with $Re = 1000, Ha = 1000, N = 51$ via Method I.

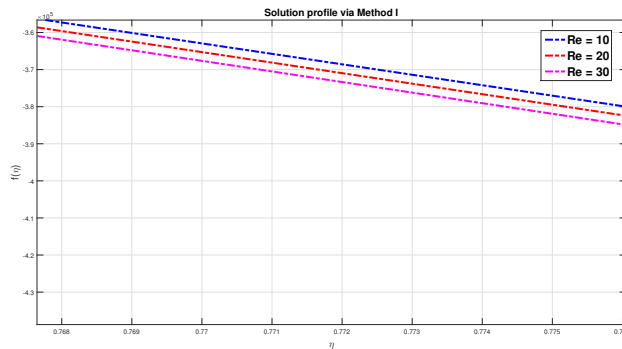


FIGURE 6. Solution profile at $Re = 10, 20, 30$ with $\alpha = -5, Ha = 1000$ via Method I.

Justification: As there is increase in the value of α (become more less negative), there is reduction in the converging effect, due to which there is broader aspect in the channel geometry. Moreover, for a strong magnetic field, turbulence is reduced which causes the overall increase in the solution profile.



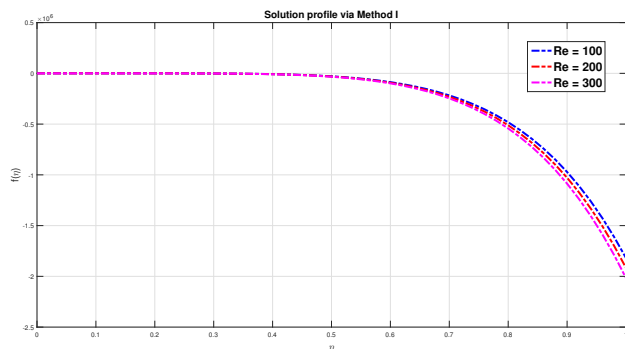


FIGURE 7. Solution profile at $Re = 100, 200, 300$ with $\alpha = -5, Ha = 1000$ via Method I.

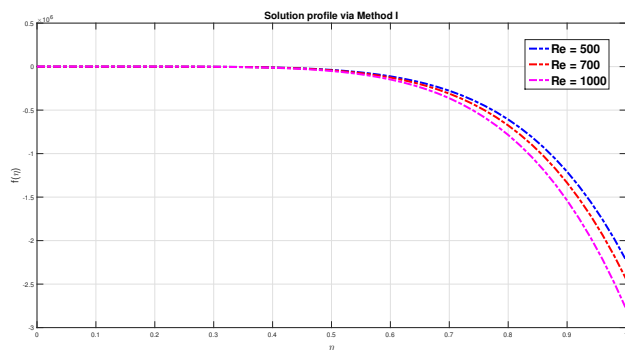


FIGURE 8. Solution profile at $Re = 500, 700, 1000$ with $\alpha = -5, Ha = 1000$ via Method I.

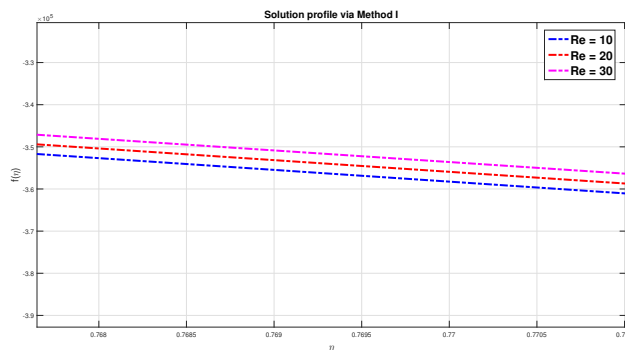


FIGURE 9. Solution profile at $Re = 10, 20, 30$ with $\alpha = 5, Ha = 1000$ via Method I.

Observation 2. Via Figures 3 and 5, it is observed that for positive α and large value of Reynold number Re and Hartmann number Ha , when there is increase in the value of α , the solution profile got decreased.



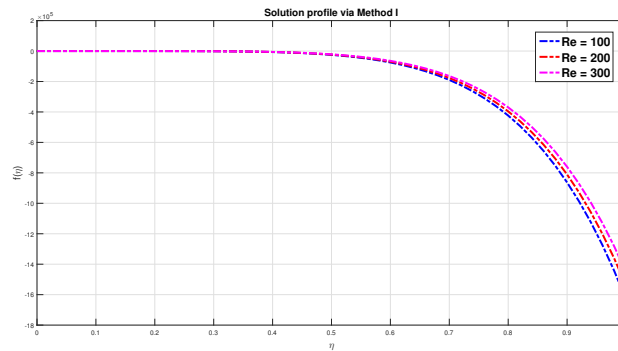


FIGURE 10. Solution profile at $Re = 100, 200, 300$ with $\alpha = 5, Ha = 1000$ via Method I.

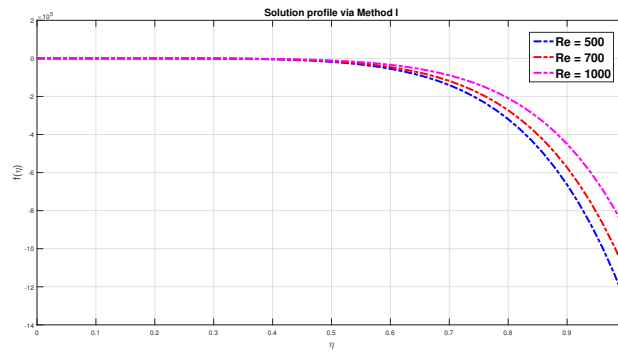


FIGURE 11. Solution profile at $Re = 500, 700, 1000$ with $\alpha = 5, Ha = 1000$ via Method I.

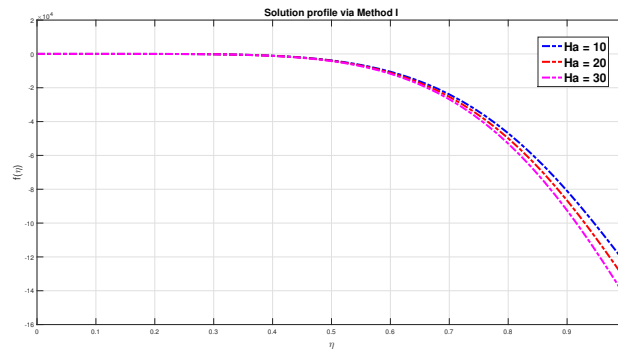


FIGURE 12. Solution profile at $Ha = 10, 20, 30$ with $\alpha = -5, Re = 1000$ via Method I.

Justification: As α is increased, there is diverging effect enhancement, which leads to reduced peak velocity and flatten the solution profile. Moreover, strong magnetic field further dampens flow, subdues instabilities but also contributes to a decrease in overall solution profile.



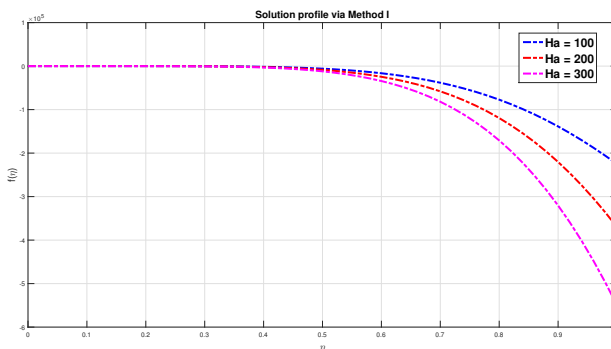


FIGURE 13. Solution profile at $Ha = 100, 200, 300$ with $\alpha = -5, Re = 1000$ via Method I.

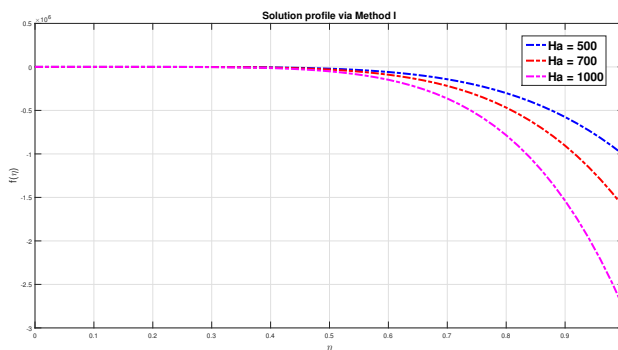


FIGURE 14. Solution profile at $Ha = 500, 700, 1000$ with $\alpha = -5, Re = 1000$ via Method I.

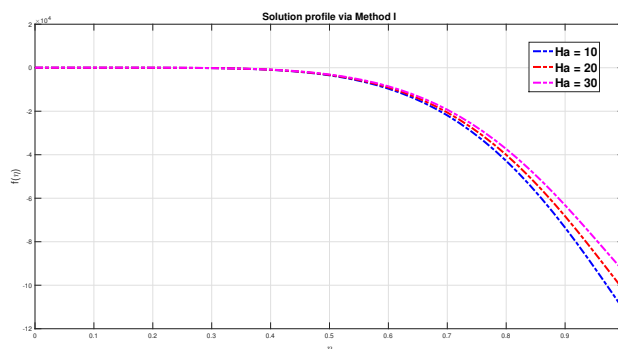


FIGURE 15. Solution profile at $Ha = 10, 20, 30$ with $\alpha = 5, Re = 1000$ via Method I.

Observation 3. Via Figures 6–8, it is noticed that for increased value of Reynolds number Re , the solution profile got decreased where α is negative and Hartmann number Ha is quite large.

Justification: When there is an increase in the value of Reynolds number, the dominance of initial forces is noticed for $(\alpha < 0)$. For a large value of Hartmann number Ha magnetic field dampens the velocity profile, so overall flow magnitude is reduced.



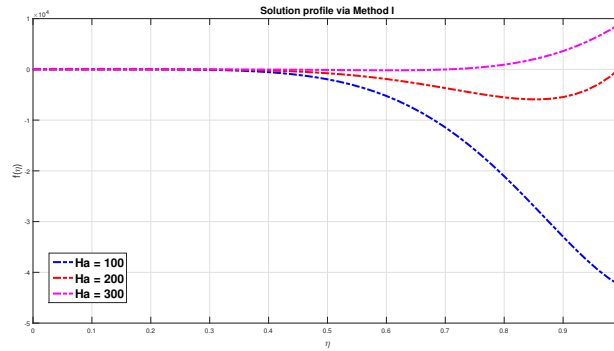


FIGURE 16. Solution profile at $Ha = 100, 200, 300$ with $\alpha = 5, Re = 1000$ via Method I.

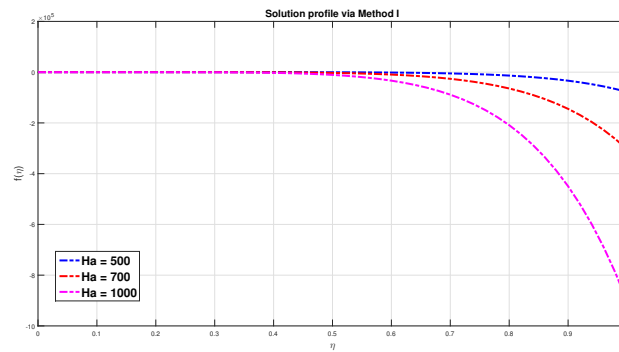


FIGURE 17. Solution profile at $Ha = 500, 700, 1000$ with $\alpha = 5, Re = 1000$ via Method I.

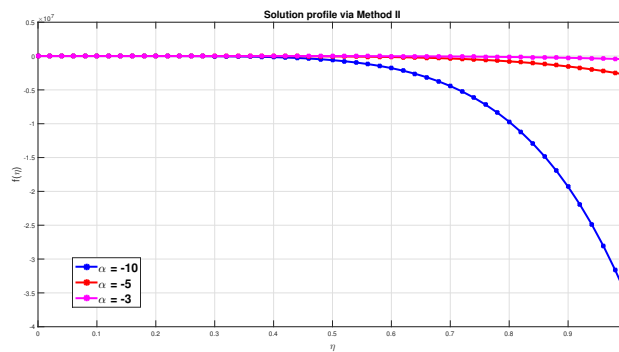


FIGURE 18. Solution profile at $\alpha = -10, -5, -3$ with $Re = 1000, Ha = 1000, N = 51$ via Method II.

Observation 4. Via Figures 9–11, increased value of Re with positive α and large Hartmann number Ha resulted into the increased solution profile.

Justification: For $\alpha > 0$ and large value of Hartmann number Ha , increasing Re enhances inertial forces, which aligns with pressure gradient, amplifying solution profile despite there is damped magnetic field.



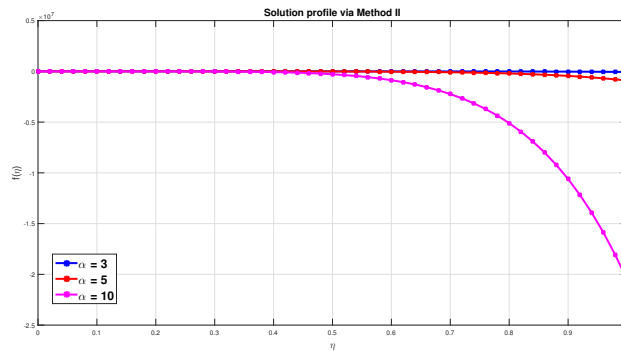


FIGURE 19. Solution profile at $\alpha = 3, 5, 10$ with $Re = 1000, Ha = 1000, N = 51$ via Method II.

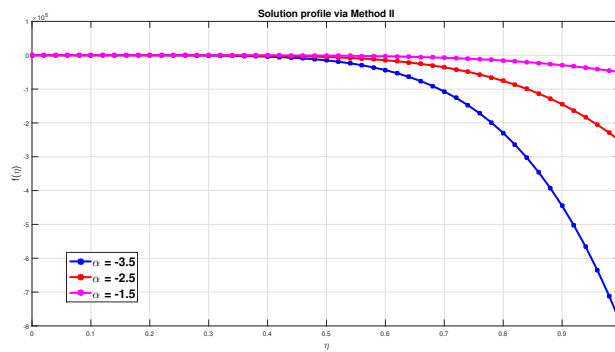


FIGURE 20. Solution profile at $\alpha = -3.5, -2.5, -1.5$ with $Re = 1000, Ha = 1000, N = 51$ via Method II.

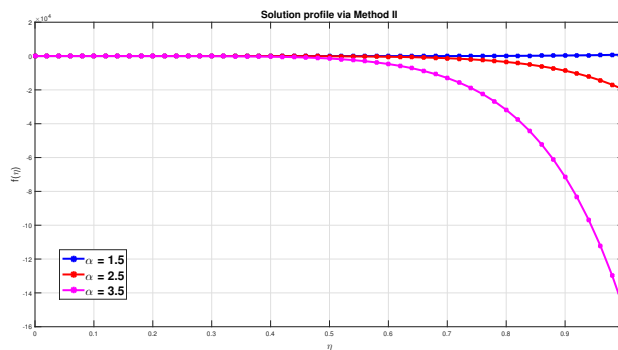


FIGURE 21. Solution profile at $\alpha = 1.5, 2.5, 3.5$ with $Re = 1000, Ha = 1000, N = 51$ via Method II.

Observation 5. Via Figures 12–14, increased value of Ha with negative α and large Reynolds number Re resulted into the decreased solution profile.

Justification: For negative $\alpha < 0$ and large value of Re , increasing Ha provides strength to magnetic damping, which opposes inertial forces and further reduce solution profile.



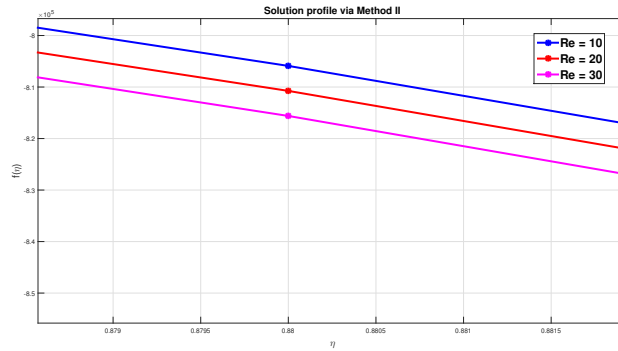


FIGURE 22. Solution profile at $Re = 10, 20, 30$ with $\alpha = -5, Ha = 1000$ via Method II.

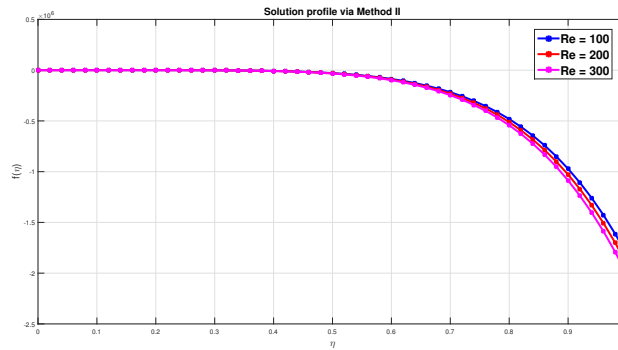


FIGURE 23. Solution profile at $Re = 100, 200, 300$ with $\alpha = -5, Ha = 1000$ via Method II.

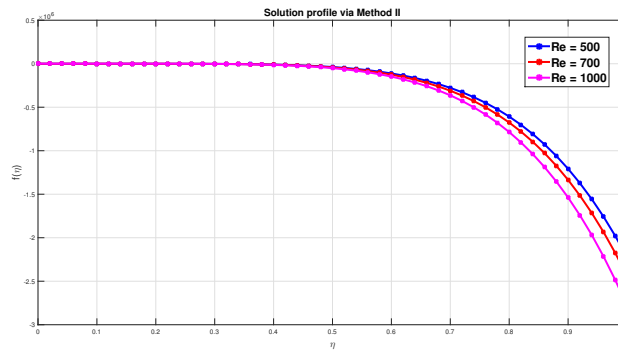


FIGURE 24. Solution profile at $Re = 500, 700, 1000$ with $\alpha = -5, Ha = 1000$ via Method II.

Observation 6. Via Figures 15–16, increased value of Ha with positive α and large Reynolds number Re resulted into the increased solution profile.

Justification: For $\alpha > 0$ and large value of Re , increasing value of Ha stabilizes flow by repressing turbulence, which allows solution profile to increase due to the dominant inertial and pressure forces.



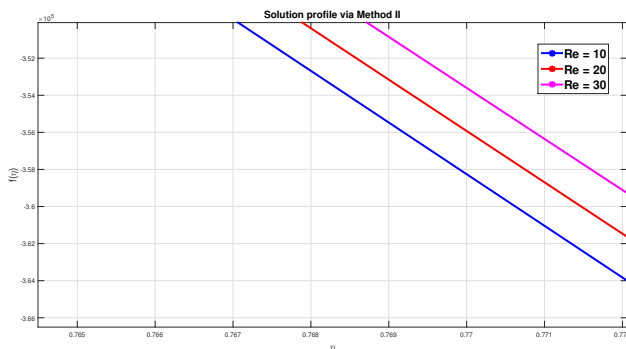


FIGURE 25. Solution profile at $Re = 10, 20, 30$ with $\alpha = 5, Ha = 1000$ via Method II.

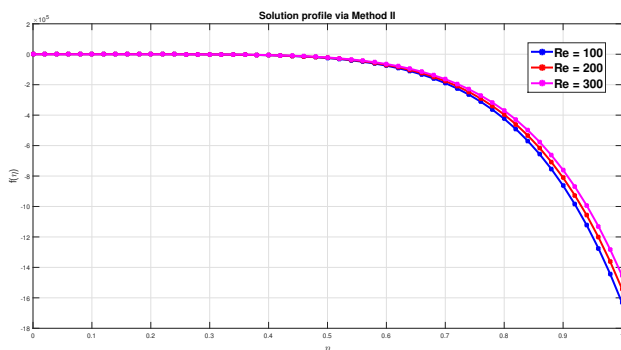


FIGURE 26. Solution profile at $Re = 100, 200, 300$ with $\alpha = 5, Ha = 1000$ via Method II.

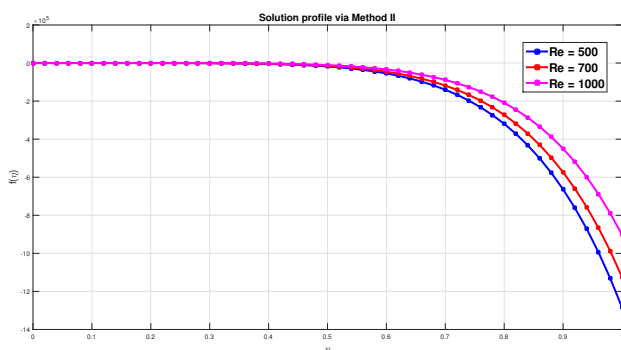


FIGURE 27. Solution profile at $Re = 500, 700, 1000$ with $\alpha = 5, Ha = 1000$ via Method II.

4. CONCLUSION

To sum up, this work presents two new semi-analytical approaches for efficiently analyzing the Jeffrey-Hamel fluid flow model's solution profiles: the Shehu-HPM and Elzaki-HPM methods. These techniques, which were created by combining the Shehu and Elzaki transforms with Homotopy Perturbation Method (HPM), show their effectiveness and dependability as novel



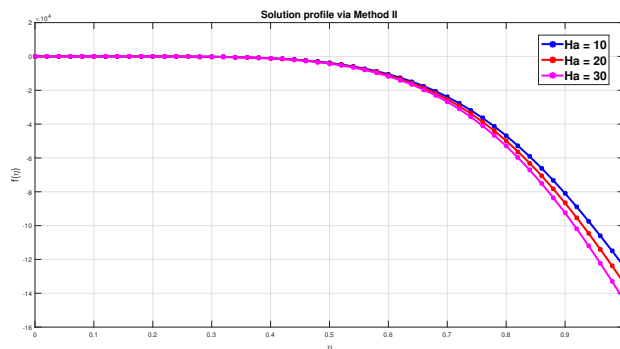


FIGURE 28. Solution profile at $Ha = 10, 20, 30$ with $\alpha = -5, Re = 1000$ via Method II.

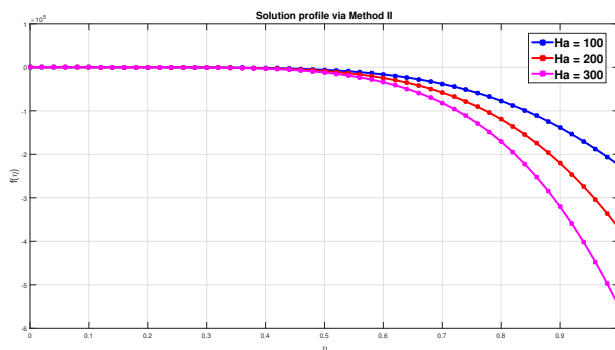


FIGURE 29. Solution profile at $Ha = 100, 200, 300$ with $\alpha = -5, Re = 1000$ via Method II.

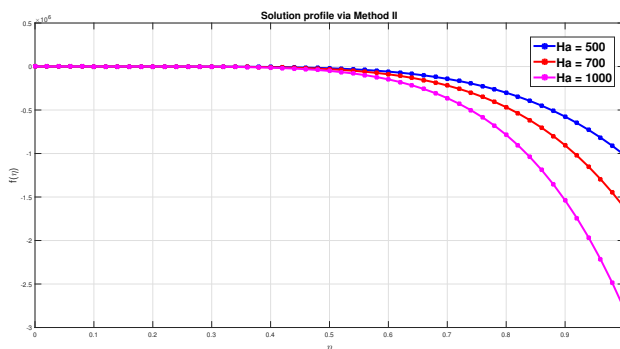


FIGURE 30. Solution profile at $Ha = 500, 700, 1000$ with $\alpha = -5, Re = 1000$ via Method II.

strategies. We assess these methods' performance under various parameters, including the Reynolds number and Hartmann number, and discover that they are not only easy to use but also error-free, unlike discretization or quasi-linearization errors. In this study, the same solutions are matched using the two strategies given. These techniques stand out as useful and adaptable instruments with a great deal of potential for applications in fluid mechanics, given the increasing demand for reliable solutions in this area. The novelties of this research lie in Hybridization of novel integration transforms with HPM and to provide a



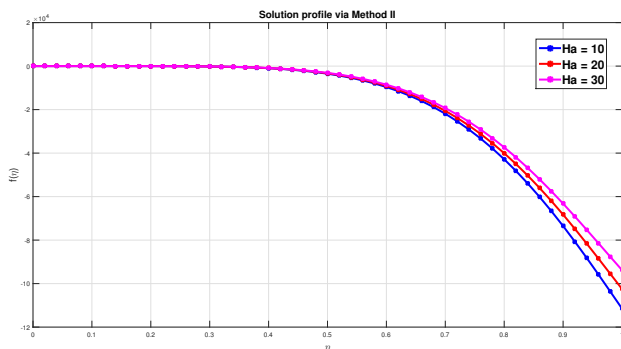


FIGURE 31. Solution profile at $Ha = 10, 20, 30$ with $\alpha = 5, Re = 1000$ via Method II.

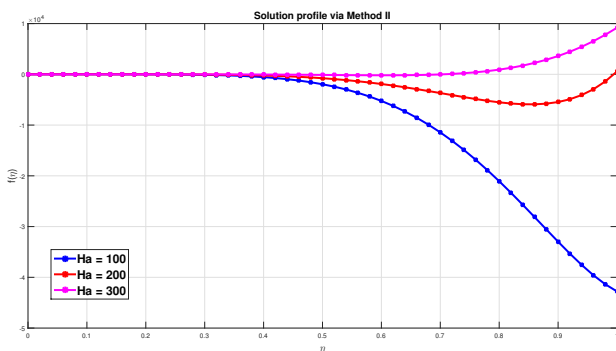


FIGURE 32. Solution profile at $Ha = 100, 200, 300$ with $\alpha = 5, Re = 1000$ via Method II.

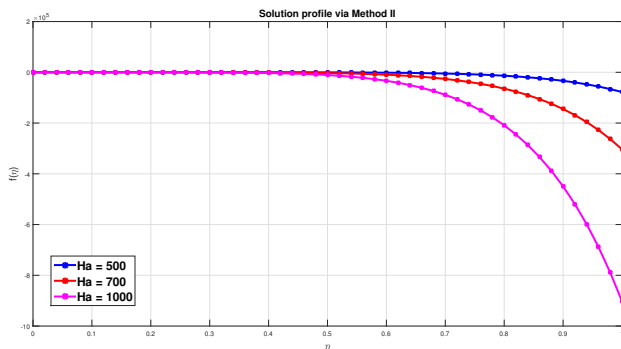


FIGURE 33. Solution profile at $Ha = 500, 700, 1000$ with $\alpha = 5, Re = 1000$ via Method II.

comparative analysis of two proposed methods. As a future scope, proposed technique will be useful to tackle a variety of fractional order fluid flow problems.

Conflict of Interest - Not applicable.

Data availability statement - Not applicable.



REFERENCES

- [1] O. Abu Arqub, *Numerical solutions for the Robin time-fractional partial differential equations of heat and fluid flows based on the reproducing kernel algorithm*, Int. J. Numer. Methods Heat Fluid Flow, 28(4) (2018), 828–856.
- [2] O. Abu Arqub, *Numerical simulation of time-fractional partial differential equations arising in fluid flows via reproducing kernel method*, Int. J. Numer. Methods Heat Fluid Flow, 30(11) (2020), 4711–4733.
- [3] O. A. Arqub and M. Al-Smadi, *Numerical solutions of Riesz fractional diffusion and advection-dispersion equations in porous media using iterative reproducing kernel algorithm*, J. Porous Media, 23(8) (2020).
- [4] O. A. Arqub and N. Shawagfeh, *Application of reproducing kernel algorithm for solving Dirichlet time-fractional diffusion-Gordon types equations in porous media*, J. Porous Media, 22(4) (2019).
- [5] W. Adel, K. E. Biçer, and M. Sezer, *A novel numerical approach for simulating the nonlinear MHD Jeffery–Hamel flow problem*, Int. J. Appl. Comput. Math., 7 (2021), 1–15.
- [6] A. Ahmed, *Jafari variation iteration method for solving one-dimensional fractional diffusion equation*, Math. Anal. Contemp. Appl., 6(1) (2024), 49–58.
- [7] Z. Alsalami, *Modeling of Optimal Fully Connected Deep Neural Network based Sentiment Analysis on Social Networking Data*, J. Smart Internet Things, 2022(1) (2023), 114–132.
- [8] F. Alsidrani, A. Kiliçman, and N. Senu, *A comprehensive review of the recent numerical methods for solving FPDEs*, Open Math., 22(1) (2024), 20240036.
- [9] Z. Asghar, R. S. Saif, and A. Z. Ghaffari, *Numerical study of boundary stresses on Jeffery–Hamel flow subject to Soret/Dufour effects*, Proc. Inst. Mech. Eng. Part C: J. Mech. Eng. Sci., 237(5) (2023), 1088–1105.
- [10] F. Aslanova, *A comparative study of the hardness and force analysis methods used in truss optimization with metaheuristic algorithms and under dynamic loading*, J. Res. Sci. Eng. Technol., 8(1) (2020), 25–33.
- [11] U. Biswal and S. Chakraverty, *Investigation of Jeffery–Hamel flow for nanofluid in the presence of magnetic field by a new approach in the optimal homotopy analysis method*, J. Appl. Comput. Mech., 8(1) (2022), 48–59.
- [12] U. Biswal, S. Chakraverty, and B. K. Ojha, *Application of homotopy perturbation method in inverse analysis of Jeffery–Hamel flow problem*, Eur. J. Mech.-B/Fluids, 86 (2021), 107–112.
- [13] A. Boudjemline, I. Ahmad, S. Rehman, Hashim, and N. B. Khedher, *Jeffery–Hamel flow extension and thermal analysis of Oldroyd-B nanofluid in expanding channel*, J. Non-Equilib. Thermodyn., 48(1) (2023), 75–90.
- [14] A. El-Shenawy, M. El-Gamel, and M. Abd El-Hady, *On the solution of MHD Jeffery–Hamel problem involving flow between two nonparallel plates with a blood flow application*, Heat Transfer, 53(6) (2024), 2905–2933.
- [15] A. C. Extra Loyinmi and T. K. Akinfe, *Exact solutions to the family of Fisher’s reaction-diffusion equation using Elzaki homotopy transformation perturbation method*, Eng. Rep., 2(2) (2020), e12084.
- [16] R. Gautam, A. Sinha, H. R. Mahmood, N. Singh, S. Ahmed, N. Rathore, and M. S. Raza, *Enhancing Handwritten Alphabet Prediction with Real-time IoT Sensor Integration in Machine Learning for Image*, J. Smart Internet Things, 2022(1) (2023), 53–64.
- [17] M. Hafeez, Hashim, and M. Khan, *Jeffery–Hamel flow of hybrid nanofluids in convergent and divergent channels with heat transfer characteristics*, Appl. Nanosci., 10 (2020), 5459–5468.
- [18] H. Haowei, U. A. R. Hussein, Z. H. Al-Qaim, F. M. Altalbawy, A. A. Fadhil, M. M. Al-Tae, and M. Hekmatifar, *Employing Sisko non-Newtonian model to investigate the thermal behavior of blood flow in a stenosis artery: Effects of heat flux, different severities of stenosis, and different radii of the artery*, Alex. Eng. J., 68 (2023), 291–300.
- [19] M. A. AL-Jawary and O. M. Salih, *Effective Computational Methods for Solving the Jeffery–Hamel Flow Problem*, Baghdad Sci. J., 20(3) (2023), 0853–0853.
- [20] A. M. Jasim, *New Analytical Study for Nanofluid between Two Non-Parallel Plane Walls (Jeffery–Hamel Flow)*, J. Appl. Comput. Mech., 7(1) (2021), 213–224.
- [21] A. Kamran, E. Azhar, N. Akmal, Z. Mehmood, and Z. Iqbal, *Finite difference approach for critical value analysis to describe Jeffery–Hamel flow toward an inclined channel with microrotations*, Arab. J. Sci. Eng., 47(12) (2022), 15261–15268.
- [22] M. Kapoor and V. Joshi, *A comparative study of Sumudu HPM and Elzaki HPM for coupled Burgers’ equation*, Heliyon, 9(5) (2023).
- [23] M. Kapoor, N. Bin Turki, and N. A. Shah, *Study of fractional telegraph equation via Shehu homotopy perturbation method*, Open Phys., 22(1) (2024), 20240029.
- [24] M. Kapoor, N. A. Shah, S. Saleem, and W. Weera, *An analytical approach for fractional hyperbolic telegraph equation using Shehu transform in one, two, and three dimensions*, Math., 10(12) (2022), 1961.
- [25] M. Kapoor, *Analytical Approach for Solution of Linear and Non-linear Time-Fractional Schrödinger’s Equations by Employing Sumudu Transform Iterative Method*, Int. J. Appl. Comput. Math., 9(3) (2023), 38.



- [26] A. S. Kelil and A. R. Appadu, *Shehu-Adomian decomposition method for dispersive KdV-type equations*, in *Mathematical Analysis and Applications: MAA 2020*, Jamshedpur, India, November 2–4, Springer Singapore, (2022), 103–129.
- [27] K. A. Kshirsagar, V. R. Nikam, S. B. Gaikwad, and S. A. Tarate, *An innovative computational approach for fuzzy space-time fractional telegraph equation via the new iterative transform method*, *Comput. Methods Differ. Equ.*, *12*(4) (2024), 763–779.
- [28] S. Kumbinarasaiah and K. R. Raghunatha, *Numerical solution of the Jeffery–Hamel flow through the wavelet technique*, *Heat Transfer*, *51*(2) (2022), 1568–1584.
- [29] S. Kumbinarasaiah, K. R. Raghunatha, and M. P. Preetham, *Applications of Bernoulli wavelet collocation method in the analysis of Jeffery–Hamel flow and heat transfer in Eyring–Powell fluid*, *J. Therm. Anal. Calorim.*, *148*(3) (2023), 1173–1189.
- [30] M. Lakestani, J. Manafian, A. R. Najafizadeh, and M. Partohaghighi, *Some new soliton solutions for the nonlinear fifth-order integrable equations*, *Comput. Methods Differ. Equ.*, *10*(2) (2022), 445–460.
- [31] M. I. Liaqat and A. Akgül, *Approximate and Exact Solutions of Some Nonlinear Differential Equations Using the Novel Coupling Approach in the Sense of Conformable Fractional Derivative*, *Contemp. Math.*, *4132–4160* (2024).
- [32] M. I. Liaqat, A. Akgül, and M. Bayram, *Series and closed form solution of Caputo time-fractional wave and heat problems with the variable coefficients by a novel approach*, *Opt. Quantum Electron.*, *56*(2) (2024), 203.
- [33] A. J. Majeed and A. Z. J. A. Nabi, *Three iterative methods for solving Jeffery–Hamel flow problem*, *Kuwait J. Sci.*, *47*(1) (2020).
- [34] J. Manafian, L. A. Dawood, and M. Lakestani, *New solutions to a generalized fifth-order KdV-like equation with prime number $p = 3$ via a generalized bilinear differential operator*, *Partial Differ. Equ. Appl. Math.*, *9* (2024), 100600.
- [35] J. Manafian and M. Lakestani, *N-lump and interaction solutions of localized waves to the $(2+1)$ -dimensional variable-coefficient Caudrey–Dodd–Gibbon–Kotera–Sawada equation*, *J. Geom. Phys.*, *150* (2020), 103598.
- [36] J. Manafian and M. Lakestani, *Application of $\tan(\phi/2)$ -expansion method for solving the Biswas–Milovic equation for Kerr law nonlinearity*, *Optik*, *127*(4) (2016), 2040–2054.
- [37] J. Manafian and M. Lakestani, *Optical soliton solutions for the Gerdjikov–Ivanov model via $\tan(\phi/2)$ -expansion method*, *Optik*, *127*(20) (2016), 9603–9620.
- [38] J. Manafian and M. Lakestani, *Abundant soliton solutions for the Kundu–Eckhaus equation via $\tan(\phi(\xi))$ -expansion method*, *Optik*, *127*(14) (2016), 5543–5551.
- [39] H. Ma, *Research on promotion of lower limb movement function recovery after stroke by using lower limb rehabilitation robot in combination with constant velocity muscle strength training*, in *2021 7th International Symposium on Mechatronics and Industrial Informatics (ISMII)*, IEEE, (2021), 70–73.
- [40] R. A. Oderimu, K. A. Salaudeen, P. I. Farayola, and W. A. Tijani, *Solution of Nonlinear Brusselator Model by a Combined Sawi Transform and Homotopy Analysis Method*, *International Conference and Advanced workshop on Modelling and Simulation of Complex Systems Department of Mathematics, Obafemi Awolowo University, Ile-Ife, Nigeri*, (2024).
- [41] D. Rezaee, A. Samari, and A. Mirsaeidi, *Heat transfer in the Jeffery–Hamel flow of a yield-stress fluid*, *Int. J. Heat Mass Transf.*, *216* (2023), 124531.
- [42] A. S. Rikani, *Investigation of turbulent fluid flow in the presence of a magnetic field induced dynamic motion of the vessel*, *J. Res. Sci. Eng. Technol.*, *9*(1) (2021), 74–94.
- [43] M. Seyyedi and A. Molajou, *Nanohydroxyapatite loaded-acrylated polyurethane nanofibrous scaffolds for controlled release of paclitaxel anticancer drug*, *J. Res. Sci. Eng. Technol.*, *9*(1) (2021), 50–61.
- [44] Vivek and M. Kumar, *Bernoulli wavelet application to the numerical solution of Jeffery–Hamel flow problem*, *Numer. Heat Transf. Part B: Fundam.*, *1–20* (2024).

